

Multidimensional Electron Transfer Pathways in a Tetrahedral Tetrakis{4-[N,N-di(4-methoxyphenyl)amino]phenyl}Phosphonium Salt: One-Step vs Two-Step Mechanism[†]

Christoph Lambert,^{*,‡} Gilbert Nöll,[‡] and Frank Hampel[§]

Institut für Organische Chemie, Julius-Maximilians-Universität Würzburg, Am Hubland, 97074 Würzburg, Germany, and Institut für Organische Chemie, Friedrich-Alexander-Universität Erlangen-Nürnberg, Henkestrasse 42, 91054 Erlangen, Germany

Received: December 15, 2000; In Final Form: April 16, 2001

Different electron-transfer pathways have been investigated in a three-dimensional redox system: tetrakis{4-[N,N-di(4-methoxyphenyl)amino]phenyl}phosphonium tetrafluoroborate $\mathbf{1}^+\mathbf{BF}_4^-$ which comprises of four triarylamine redox centers arranged in a pseudo-tetrahedral geometry. Using a UV/Vis/NIR spectroelectrochemical setup we generated the mixed-valence species $\mathbf{1}^{2+}$, $\mathbf{1}^{3+}$, and $\mathbf{1}^{4+}$ and measured the UV/Vis/NIR spectra. These spectra were analyzed and interpreted according to a multi-dimensional Marcus–Hush approach. The analysis revealed that both the photoexcited as well as the thermal ET in $\mathbf{1}^{3+}$ are forbidden as a concerted two-electron transfer but allowed as two consecutive one-electron transfer steps.

Introduction

The purpose of this paper is to elucidate different possible electron transfer (ET) pathways in a three-dimensional phosphonium ion with four triarylamine redox centers arranged in a pseudo-tetrahedral manner.

Most of the artificial ET model systems consist of a linear sequence of two or more redox centers separated by saturated or unsaturated spacers.¹ These redox cascades may be termed dyades, triades, tetraades, etc. according to the number of redox centers involved. The spacers serve to mediate the ET by a so-called super exchange mechanism where the electron (or hole) is never localized vibronically at the bridge.² While for studying photoinduced ET processes different (neutral) donor and acceptor centers are combined, two donor (or acceptor) centers may be connected to study degenerate mixed valence systems where one of the donors (acceptors) is oxidized (reduced) and serves as the electron acceptor (donor). These mixed valence systems have been widely explored in inorganic and organometallic chemistry,³ however, the number of purely organic systems studied so far is relatively small.⁴ Even less attention has been paid to both organic and inorganic mixed valence systems which possess a branched structure and three or more redox centers which are related by symmetry operations.⁵ Because of their branched nature, these systems display more than one ET pathway. One of the most prominent natural ET systems is the photosynthetic reaction center of *Rhodospseudomonas viridis* whose three-dimensional structure is known in great detail.⁶ In this reaction center, two redox cascades (M and L branch) each consisting of a bacteriochlorophyll–bacteriochlorophyll–bacteriopheophytin–quinone tetrad are related by an

approximate C_2 axis. Although superficially identical, the ET occurs in only one of these cascades, the L branch, because of small reaction enthalpy differences between L and M branch for the first ET step in the redox cascade. This example demonstrates that the investigation of multidimensional ET processes related by symmetry is of prime interest.

Marcus theory has been employed for the theoretical description of one-dimensional ET processes with great success.⁷ According to this concept, the adiabatic ET energy hypersurfaces can be constructed from two parabolic diabatic functions, each representing a (noninteracting) state where the electron is localized at the left (right) hand side of the molecule, by solving a 2×2 secular equation.⁸ The energy splitting of the adiabatic surfaces at the (avoided) crossing point of the two diabatic potentials is twice the coupling integral V whose magnitude is a measure for the electronic interaction of the two diabatic states. In contrast to the simple Marcus theory for weakly adiabatic ET where the thermal barrier of a degenerate ET process is $\lambda/4$, one has to calculate ΔG^* for strongly adiabatic ($V \gg k_B T$) cases from eq 1 with λ being the total Marcus reorganization energy.

$$\Delta G^* = \frac{\lambda}{4} - V + \frac{V^2}{\lambda} \quad (1)$$

Again, little work has been done to adopt Marcus theory for multidimensional ET pathways. Grunwald⁹ as well as Guthrie¹⁰ used quadratic and quartic functions to model the ground state potential surface of two- and multi-dimensional reaction pathways directly without solving a secular equation. Although these models were mainly derived for proton transfer reactions they equally apply to ET processes.¹¹ In this paper, we want to exemplify how the two-state model can be used for constructing the adiabatic energy potential surfaces of a three-dimensional ET system and how to analyze spectroelectrochemical measurements to evaluate V in this case. We used the tetrakis{4-[N,N-di(4-methoxyphenyl)amino]phenyl}phosphonium cation $\mathbf{1}^+$ as a practically tetrahedral species with four triarylamine redox

[†] Dedicated to Prof. Dr. h. c. mult. Siegfried Hünig on the occasion of his 80th birthday.

* To whom correspondence should be addressed. E-mail: lambert@chemie.uni-wuerzburg.de; fax: 0049(0)931 888 4606

[‡] Julius-Maximilians-Universität Würzburg.

[§] Friedrich-Alexander-Universität Erlangen-Nürnberg.

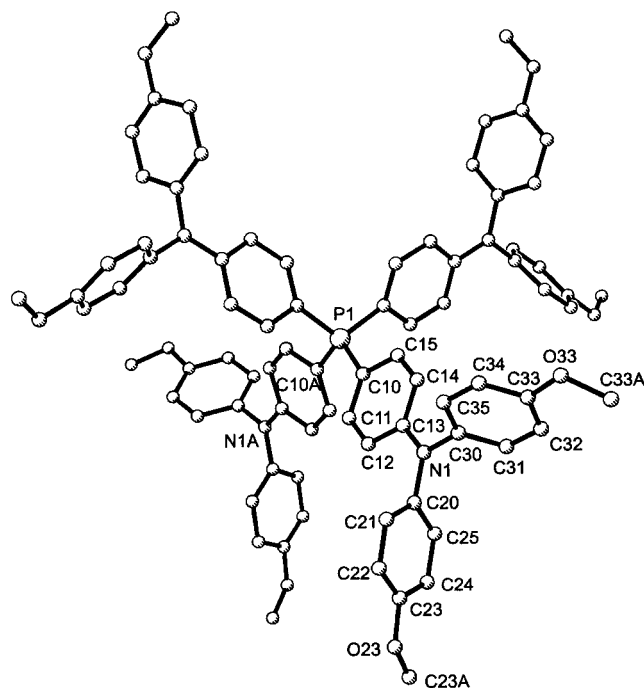
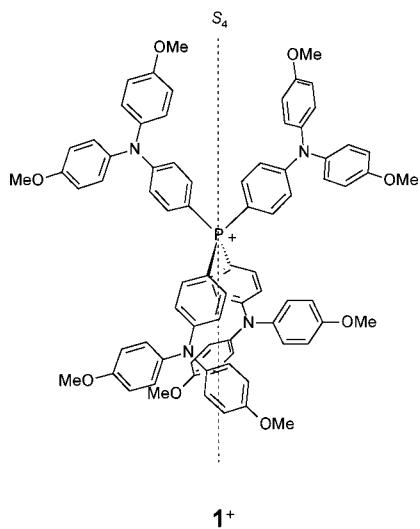


Figure 1. X-ray structure of 1^+ . Hydrogen atoms and counterion omitted for clarity. Molecular point group S_4 . Selected distances and angles: P1–C10 1.780(4), C10–C11 1.392(6), C11–C12 1.373(6), C12–C13 1.397(6), C13–C14 1.398(5), C14–C15 1.351(6), C10–C15 1.433(6), N1–C13 1.379(5), N1–C30 1.426(6), N1–C20 1.440(5), C10–P1–C10A 111.2(3), C13–N1–C20 122.5(4), C13–N1–C30 121.9(3), C20–N1–C30 115.6(3).

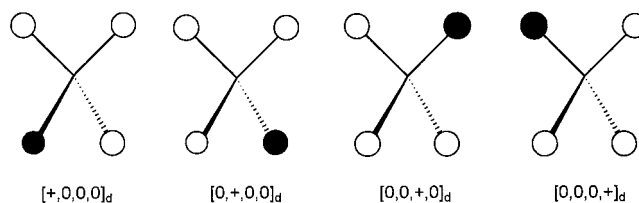
centers which may exist in three different mixed valence states. The triarylamine centers were chosen so as to ensure reversible oxidation and because of their importance as hole carriers in optoelectronic materials¹² and their interesting magnetic properties.¹³ For these reasons, Bonvoisin et al. and we have used oligotriarylamine systems to investigate their mixed valence and intramolecular ET properties in the past.^{4q,5c–f}



Results and Discussion

The Structure of 1^+ . An X-ray crystallographic investigation of a single crystal of $1^+BF_4^-$ gave a tetragonal space group I_1/a with the 1^+ ions adopting crystallographic S_4 symmetry (see Figure 1). Although the nitrogens are almost tetrahedrally

CHART 1



arranged around the phosphorus center (N–N distances are $4 \times 9.45 \text{ \AA}$ and $2 \times 10.27 \text{ \AA}$, the medium effective ET distance thus is 9.72 \AA), S_4 is the highest symmetry possible because the propeller-like structure of the triarylamine moieties (angle sum around N = 360°) destroys the C_3 axis necessary for true T symmetry. However, for the ET processes it is the relative orientation of the triarylamine moieties and the nitrogen lone-pair orbitals which is important. When oxidized to the dication 1^{2+} or to the tetracation 1^{4+} the highest symmetry possible then is C_1 and when oxidized to the trication 1^{3+} it is C_2 . However, as the structural changes between a neutral triarylamine and its radical cation are only minor¹⁴ we can safely assume approximate S_4 symmetry for the geometry of 1^{2+} , 1^{3+} , and 1^{4+} . In addition, as will be explained in the computational section, 1^+ behaves as if it had T geometry concerning its ET properties. The phenylene rings bound between N and P show a slight distortion toward a quinoid structure which is due to the push–pull character of the substituents.

The Theoretical Model

The Diabatic and Adiabatic States of 1^{2+} and 1^{4+} . Oxidation of 1^+ can yield the radical dication 1^{2+} , diradical trication 1^{3+} , triradical tetracation 1^{4+} , and the fully oxidized tetradical pentacation 1^{5+} . The ions 1^{2+} , 1^{3+} , and 1^{4+} are mixed valence species which might display degenerate ET processes. If one ignores different spin eigenstates of the triradical 1^{4+} the transfer of a hole in 1^{2+} is equivalent to the transfer of an electron in 1^{4+} . Henceforth, we will discuss the properties of 1^{2+} only. There are four diabatic states of 1^{2+} where the hole is localized in one of the four triarylamine centers. The four diabatic states (in their electronic ground state) can be labeled by $[+0,0,0]_d$, $[0,+0,0]_d$, $[0,0,+0]_d$, and $[0,0,0+]_d$ where 0 and + denotes the charge localized at a given triarylamine moiety and the index d stands for diabatic (Chart 1). The energy of these states is a function of the ET coordinates. Owing to the approximate S_4 geometry of 1^+ , there are two electronic couplings V_1 and V_2 between these diabatic states. However, as will be evident in the computational section, these couplings are almost equal ($V_1 \approx V_2$).

$$\begin{vmatrix} H[+0,0,0]_d - \epsilon & V_1 & V_2 & V_2 \\ V_1 & H[0,+0,0]_d - \epsilon & V_2 & V_2 \\ V_2 & V_2 & H[0,0,+0]_d - \epsilon & V_1 \\ V_2 & V_2 & V_1 & H[0,0,0+]_d - \epsilon \end{vmatrix} = 0 \quad (2)$$

Solving the 4×4 secular equation (eq 2) with $V_1 = V_2 = V$ for these four diabatic states yields four adiabatic states whose energy again depends on the ET coordinates. These adiabatic states in their minimum ground-state geometry can be represented by the corners of a regular tetrahedron (Chart 2). We label these states by $[c^+,n^0,n^0,n^0]_a$, $[n^0,c^+,n^0,n^0]_a$, $[n^0,n^0,c^+,n^0]_a$, and $[n^0,n^0,n^0,c^+]_a$ where c and n denote triarylamine centers in the cation and neutral geometry, respectively, + and 0 denote

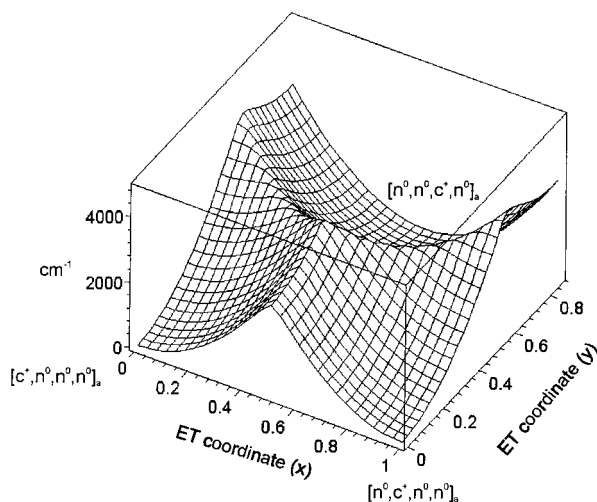
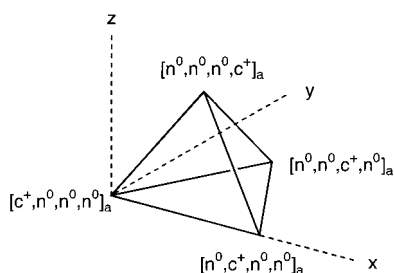


Figure 2. Potential energy surface for the ET process in 1^{2+} (or 1^{4+}).

CHART 2



the charge of the centers, and a stands for adiabatic. Moving from the starting point $[c^+, n^0, n^0, n^0]_a$ along the edges of the tetrahedron leads over the transition state of the thermal ET process to one of the other corners.

In Figure 2 the potential energy surface for a two-dimensional cut (x, y side of the tetrahedron, $z = 0$) between $[c^+, n^0, n^0, n^0]_a$, $[n^0, c^+, n^0, n^0]_a$, and $[n^0, n^0, c^+, n^0]_a$ is plotted as calculated from the lowest energy solution of eq 2 if parabolas (eq 3) are used for the diabatic potentials:^{15,16} The ET coordinates are given within a Cartesian system. Thus, coordinate x transforms $[c^+, n^0, n^0, n^0]_a$ into $[n^0, c^+, n^0, n^0]_a$, but for the transformation of $[n^0, c^+, n^0, n^0]_a$ into, e.g., $[n^0, n^0, c^+, n^0]_a$, two coordinates x and y are necessary within a Cartesian system.

$$\begin{aligned}
 H[+,0,0,0]_d &= \lambda(x^2 + y^2 + z^2) \\
 H[0,+,0,0]_d &= \lambda[(1-x)^2 + y^2 + z^2] \\
 H[0,0,+,0]_d &= \lambda\left[\left(\frac{1}{2}-x\right)^2 + \left(\frac{\sqrt{3}}{2}-y\right)^2 + z^2\right] \\
 H[0,0,0,+]_d &= \lambda\left[\left(\frac{1}{2}-x\right)^2 + \left(\frac{1}{2\sqrt{3}}-y\right)^2 + \left(\frac{\sqrt{3}}{2}-z\right)^2\right]
 \end{aligned} \quad (3)$$

Alternatively to the thermal way, an optical ET can be induced by exciting an adiabatic ground state, e.g., $[c^+, n^0, n^0, n^0]_a$,

$$\begin{vmatrix}
 H[+,+,0,0]_d - \epsilon & V_1 & V_2 & V_2 & V_1 & 0 \\
 V_1 & H[+,0,+,0]_d - \epsilon & V_3 & V_3 & 0 & V_1 \\
 V_2 & V_3 & H[+,0,0,+]_d - \epsilon & 0 & V_3 & V_2 \\
 V_2 & V_3 & 0 & H[0,+,+,0]_d - \epsilon & V_3 & V_2 \\
 V_1 & 0 & V_3 & V_3 & H[0,+,0,+]_d - \epsilon & V_1 \\
 0 & V_1 & V_2 & V_2 & V_1 & H[0,0,+,+]_d - \epsilon
 \end{vmatrix} = 0 \quad (4)$$

to its Franck–Condon state (intervalence charge-transfer, IV-CT). Thus, one has to solve again eq 2 but with the energies of the diabatic states referring to the ground-state geometry of the adiabatic state $[c^+, n^0, n^0, n^0]_a$: i.e., $H[c^+, n^0, n^0, n^0]_d = 0$, $H[c^0, n^+, n^0, n^0]_d = \lambda$, $H[c^0, n^0, n^+, n^0]_d = \lambda$, and $H[c^0, n^0, n^0, n^+]_d = \lambda$. We refrained from searching this adiabatic minimum geometry as this is quite laborious.¹⁷ Instead, we used the geometry of the diabatic minimum $[c^+, n^0, n^0, n^0]_d$ which is quite similar to the adiabatic minimum. This procedure is a good approximation in the weak coupling regime only as the minima of the adiabatic surface, e.g., $[c^+, n^0, n^0, n^0]_d$, deviate from those of the diabatic functions, e.g., $[c^+, n^0, n^0, n^0]_a$, with increasing V . The energy level diagram resulting from solving eq 2 at the fixed ground-state geometry of, e.g., $[c^+, n^0, n^0, n^0]_d$, is given in Figure 3.

There is a set of degenerate excited E states and one A state. There is no simple way to label these adiabatic states as they are delocalized. The degeneracy of excited E states is due to the (approximate) equality of all coupling integrals between the four diabatic states of the dication. It is impossible to tell anything concrete about the relative transition moments from the ground to the E and A states a priori without imposing a certain symmetry. However, in the weak coupling limit, the sum of oscillator strength to the E states and the A state is three times that of a hypothetical model compound with only two diabatic functions with the same geometrical and electronic structure (e.g., bis{4-[*N,N*-di(4-methoxyphenyl)amino]phenyl}-diphenylphosphonium cation).

The Diabatic and Adiabatic States of 1^{3+} . Again we disregard the fact that the biradical 1^{3+} can adopt two spin multiplicities (singlet and triplet). There are six diabatic states of 1^{3+} where two holes are localized in two of the four triarylamine centers. These six diabatic states (in their electronic ground state) can be labeled by $[+,+,0,0]_d$, $[+,0,+,0]_d$, $[+,0,0,+]_d$, $[0,+,+,0]_d$, $[0,+,0,+]_d$, and $[0,0,+,+]_d$ (see Chart 3).

Owing to the C_2 symmetry of 1^{3+} , the 6×6 secular equation (eq 4) for coupling these six diabatic states has three different coupling elements (V_1 , V_2 , and V_3). The matrix elements coupling those states which do not share any common oxidized site vanish because the acting operator is a one-electron operator. The same arguments for the coupling in 1^{2+} hold true for 1^{3+} which makes $V_1 \approx V_2 \approx V_3$. Solving the secular equation with the six diabatic states and with $V_1 = V_2 = V_3 = V$ results in six adiabatic states. These adiabatic states in their ground-state geometry can be represented by the corners of an octahedron (Chart 4) with the corners labeled $[c^+, c^+, n^0, n^0]_a$, $[c^+, n^0, c^+, n^0]_a$, $[c^+, n^0, n^0, c^+]_a$, $[n^0, c^+, c^+, n^0]_a$, $[n^0, c^+, n^0, c^+]_a$, and $[n^0, n^0, c^+, c^+]_a$. Moving from the starting point $[c^+, c^+, n^0, n^0]_a$ along the edges of the octahedron leads over the transition state of the thermal ET process to one out of four neighboring corners. In Figure 4, the energy potential surface for a two-dimensional section (middle square plane) between $[c^+, c^+, n^0, n^0]_a$, $[c^+, n^0, c^+, n^0]_a$, $[n^0, c^+, n^0, c^+]_a$, and $[n^0, n^0, c^+, c^+]_a$ is plotted as calculated from

CHART 3

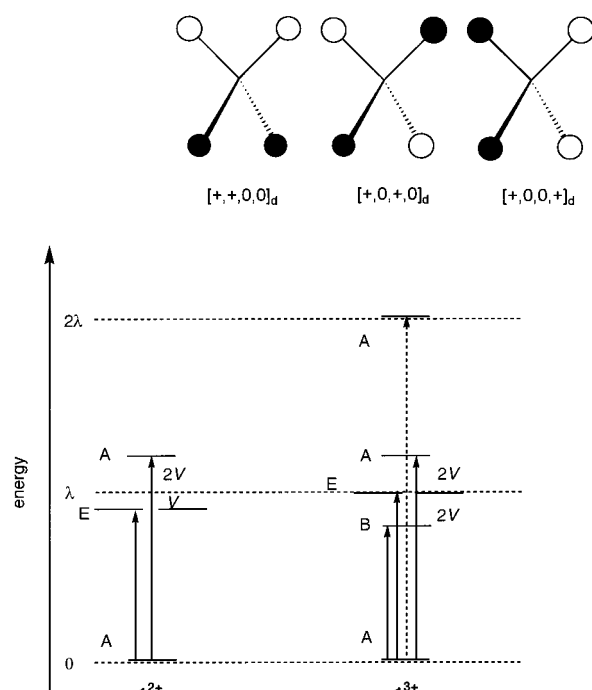


Figure 3. Energy level diagram of the excited IV-CT states of 1^{2+} and 1^{3+} . The energy splitting V is exaggerated for clarity. The dotted arrow indicates a forbidden transition.

the lowest energy solution of eq 4 with $z = 0$. Again, for the diabatic potentials parabolas were used:¹⁶

$$H[+, +, 0, 0]_d = \lambda(x^2 + y^2 + z^2)$$

$$H[+, 0, +, 0]_d = \lambda[(1-x)^2 + y^2 + z^2]$$

$$H[0, +, 0, +]_d = \lambda[x^2 + (1-y)^2 + z^2]$$

$$H[0, 0, +, +]_d = \lambda[(1-x)^2 + (1-y)^2 + z^2]$$

$$H[+, 0, 0, +]_d = \lambda\left[\left(\frac{1}{2}-x\right)^2 + \left(\frac{1}{2}-y\right)^2 + \left(\frac{1}{\sqrt{2}}-z\right)^2\right]$$

$$H[0, +, +, 0]_d = \lambda\left[\left(\frac{1}{2}-x\right)^2 + \left(\frac{1}{2}-y\right)^2 + \left(-\frac{1}{\sqrt{2}}-z\right)^2\right]$$

In contrast to 1^{2+} where moving from one corner of the tetrahedron to one of the others refers to a one-dimensional ET pathway, there exist, in principle, two alternatives in 1^{3+} for moving from $[c^+, c^+, n^0, n^0]_a$ to $[n^0, n^0, c^+, c^+]_a$: a stepwise mechanism over $[c^+, n^0, c^+, n^0]_a$, $[c^+, n^0, n^0, c^+]_a$, $[n^0, c^+, c^+, n^0]_a$, or $[n^0, c^+, n^0, c^+]_a$ as corner intermediates, each step being a one-dimensional ET, or, alternatively, a two-dimensional pathway directly along the diagonal of one of the two possible square sections. As can be seen from Figure 4, the latter mechanism leads over a hill top rather than a saddle point, i.e., *this mechanism is thermally forbidden*.

The principle aspects of the adiabatic hypersurfaces in Figures 2 and 4 could also be obtained by using the equations given by Guthrie.¹⁰ However, while Guthrie's equations were not derived by solving a secular equation, they do not take into account the influence of the electronic coupling V on the shape of the surface around and the energy at the transition states (TS). Especially around TS, Guthrie's equations give rather smooth curvatures much the same as for the minima. In contrast, modeling the

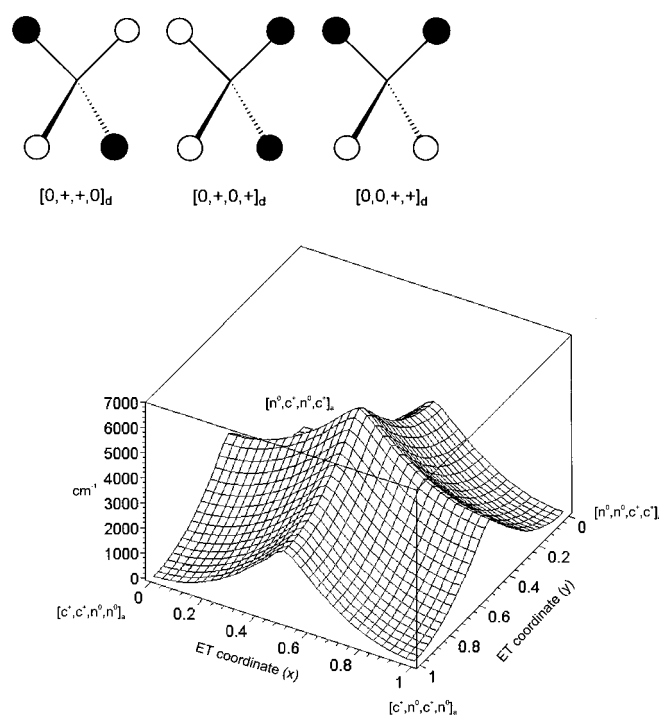


Figure 4. Potential energy surface for the ET process in 1^{3+} .

CHART 4

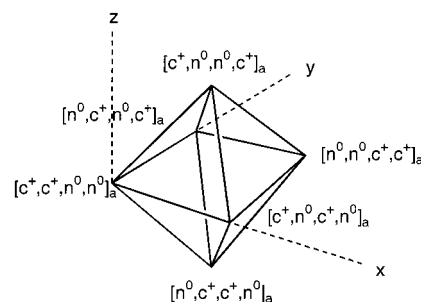
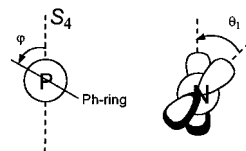


CHART 5



hypersurface from, e.g., eqs 2 and 4, gives potentials with the accurate curvature around TS depending on V . In the plots of Figures 2 and 4, we used $\lambda = 11800 \text{ cm}^{-1}$ and $V = 260 \text{ cm}^{-1}$ which were derived from analysis of the experimental UV/Vis/NIR spectra (see next section).

The state diagram for optical ET in 1^{3+} can be constructed with eq 4 analogously to 1^{2+} ; the energies of the diabatic states referring to the ground-state geometry of $[c^+, c^+, n^0, n^0]_d$ are $H[c^+, c^+, n^0, n^0]_d = 0$, $H[c^+, c^0, n^+, n^0]_d = \lambda$, $H[c^+, c^0, n^0, n^+]_d = \lambda$, $H[c^0, c^+, n^+, n^0]_d = \lambda$, $H[c^0, c^+, n^0, n^+]_d = \lambda$, and $H[c^0, c^0, n^+, n^+]_d = 2\lambda$. The energy level diagram resulting from solving eq 4 at the fixed ground-state geometry of, e.g., $[c^+, c^+, n^0, n^0]_d \approx [c^+, c^+, n^0, n^0]_a$ is given in Figure 4.¹⁷ Besides the A ground state the solution gives a set of excited degenerate E states at λ , one B state at $\lambda - 2V$, and one A states at $\lambda + 2V$ as well as a higher lying A state at $\sim 2\lambda$. The degeneracy of the E states within molecular C_2 point group is due to the approximation that all

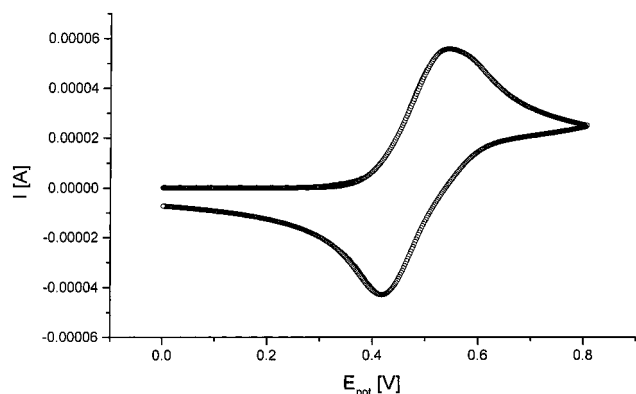


Figure 5. Cyclic voltammogram of 1^+ in $\text{CH}_2\text{Cl}_2/0.1$ M TBAH: exp. data solid line, fitted data open circles.

TABLE 1: Redox Potentials of 1^+ Measured by Cyclic Voltammetry in $\text{CH}_2\text{Cl}_2/0.1$ M TBAH and Digital Simulation as Well as for a Theoretical Model with Noninteracting Redox Centers

E_m	exp/digit simulation ^a	theor/noninteracting
$E_1 [1^+/1^{2+}]$	0.438	0.449
$E_2 [1^{2+}/1^{3+}]$	0.473	0.475
$E_3 [1^{3+}/1^{4+}]$	0.486	0.495
$E_4 [1^{4+}/1^{5+}]$	0.541	0.521

^a ± 2 mV

coupling elements are equal. In the weak coupling regime, the sum of oscillator strengths to the B, E, and A states around λ is 4/3 that of the excitation to the E and A state in 1^{2+} while that to the A state at 2λ is forbidden as a one-photon process.

Electrochemical and Spectroelectrochemical Investigations. The cyclic voltammogram (CV) of 1^+ in $\text{CH}_2\text{Cl}_2/0.1$ M TBAH displays a single unresolved wave for the reversible oxidation series: $1^+ \rightarrow 1^{2+} \rightarrow 1^{3+} \rightarrow 1^{4+} \rightarrow 1^{5+}$. Digital simulation (Figure 5) of the CV gave the four redox potentials for the four redox couples (Table 1).

The fitted potentials deviate from the values expected for noninteracting redox centers¹⁸ slightly but significantly and indicate some interaction between the triarylamine branches. UV/Vis/NIR spectra of 1^+ to 1^{5+} were monitored during stepwise electrochemical oxidation using an optically transparent thin-layer cell (ca. 100 μm) with a gold minigrad working electrode.¹⁹ The UV/Vis/NIR spectra of all the radical cations are mainly characterized by an intense band at 800 nm. The radical cations 1^{2+} , 1^{3+} , and 1^{4+} show a very weak and broad band as a shoulder at ca. 850 nm which we assign to an intervalence charge transfer (IV–CT) excitation (Figure 6). The analysis of this band is based on the assumption that the reorganization energy $\lambda = \tilde{\nu}_{\text{max}}$ is the same in 1^{2+} , 1^{3+} , and 1^{4+} and that $V(1^{2+})$, $V(1^{3+})$, and $V(1^{4+})$ are equal. This assumption is justified as the coupling is within the weak regime and the geometry differences between 1^{2+} and 1^{3+} are supposed to be minor. In addition, Bonvoisin et al.^{5c,d} found quite similar couplings for the mono and dication of a 1,3,5-tris(triarylamine) substituted benzene. As we will show in the computational part, we assume these couplings to be positive. For determining the exact energy and absorbance, we fitted this IV–CT band by a single Gaussian function under the restraint that the bandwidth at half-height at the high-temperature limit should obey eq 6²⁰ for a weakly coupled Robin-Day class II derivative:²¹

$$\tilde{\nu}_{1/2}(\text{HTL}) = 47.94\sqrt{\tilde{\nu}_{\text{max}}} \quad (6)$$

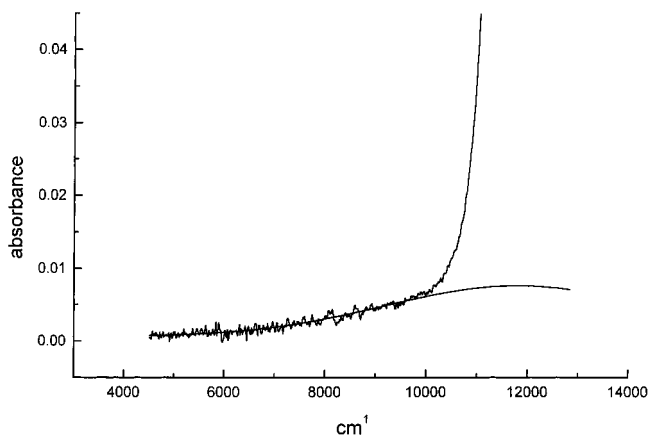


Figure 6. IV–CT band and Gaussian fit at maximal absorbance during oxidation of 1^+ .

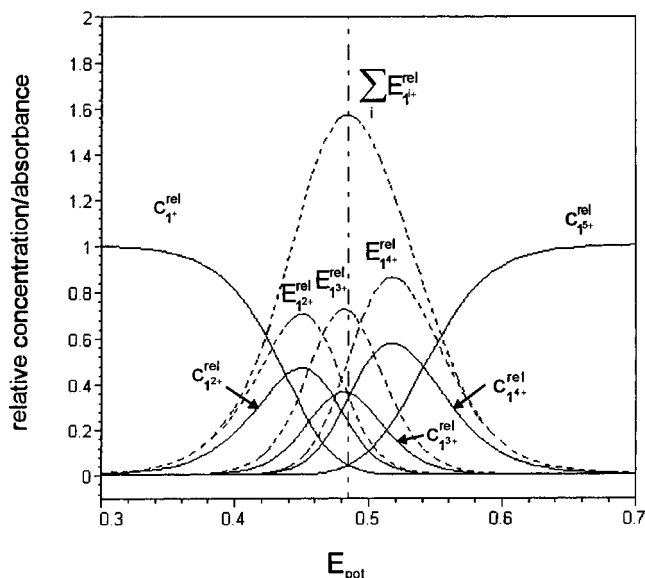


Figure 7. Relative concentrations c_{i+}^{rel} and relative absorbance E_{i+}^{rel} of 1^+ vs applied potential.

This fit gave $\tilde{\nu}_{\text{max}} = 11800 \text{ cm}^{-1}$ at a bandwidth of 5210 cm^{-1} . The IV–CT band again disappears when 1^{4+} is further oxidized to 1^{5+} and refers to an excitation from the A ground state to the excited E and A states (see Figure 3) in 1^{2+} and 1^{4+} and to an excitation from the A ground state to the B, E, and A states in 1^{3+} . As all these excitations have approximately the same energy,^{5c,d} there is only one band visible in the spectroelectrochemical experiment which comprises the IV–CT bands of 1^{2+} , 1^{3+} , and 1^{4+} whose relative concentrations in the cell depend on the standard redox potentials (see Table 1) and the electric potential applied to the working electrode.²²

According to the Mulliken–Hush treatment of IV–CT bands, we calculated the electronic coupling integral from eq 7 where r is the effective ET distance taken as the mean distance between two nitrogens $d_{\text{NN}} = 9.75 \text{ \AA}$ and μ_{eg} is the transition moment connecting the ground and the IV–CT state.^{8,20,23,24} The latter can be calculated from the integrated IV–CT absorption spectrum with eq 8 taking into account the relative molar absorptivities ϵ_i^{rel} of 1^{2+} , 1^{3+} , and 1^{4+} . s is a symmetry factor^{5c} which is 3 for 1^{2+} and 1^{4+} and 4 (\cong numbering of coupling elements V in the first row of secular eqs 2 and 4) for 1^{3+} and takes into account that a IV–CT transition is three times likelier in 1^{2+} and four times likelier in 1^{3+} than in a one-dimensional model compound. Thus, the $1/\sqrt{s}$ factor brings the couplings

of systems with different dimensionality on a common basis.

$$V = \frac{\mu_{\text{eg}}}{\sqrt{s}} \cdot \frac{\tilde{\nu}_{\text{max}}}{e \cdot r} \quad (7)$$

$$\mu_{\text{eg}} = 0.09584 \sqrt{\frac{\int \epsilon(\tilde{\nu}) d\tilde{\nu}}{\tilde{\nu}_{\text{max}}}} \quad (8)$$

For the evaluation of the electronic coupling V it is necessary to deconvolute the apparent IV–CT band into the contributions of $\mathbf{1}^{2+}$, $\mathbf{1}^{3+}$, and $\mathbf{1}^{4+}$ according to the relative concentrations present. Using the redox potentials from the digital simulation we calculated the relative concentrations $c_{i^{++}}^{\text{rel}}$ of all species depending on the electric potential by using eq 9 which was derived from coupling the Nernst equation for four redox couples. The result is plotted in Figure 7.

$$[\mathbf{1}^{i^{++}}] = \frac{[\mathbf{1}]_0 \prod_{m=1}^i \left[\exp\left(\frac{F(E - E_m)}{RT}\right) \right]}{\sum_{k=1}^5 \left\{ \prod_{m=1}^k \left[\exp\left(\frac{F(E - E_m)}{RT}\right) \right] \right\}}$$

with $i = 1 \dots 5$

$$E_1 = E, E_2 = E_{1/2}(\mathbf{1}^+/\mathbf{1}^{2+}) \dots E_5 = E_{1/2}(\mathbf{1}^{4+}/\mathbf{1}^{5+})$$

$$[\mathbf{1}]_0 = \sum_{i=1}^5 [\mathbf{1}^{i^{++}}] \quad (9)$$

Multiplying the concentration of $\mathbf{1}^{2+}$, $\mathbf{1}^{3+}$, and $\mathbf{1}^{4+}$ (only those species display an IV–CT absorption) with the relative absorptivities $\epsilon_{1^{2+}}^{\text{rel}} = \epsilon_{1^{4+}}^{\text{rel}} = 3$ and $\epsilon_{1^{3+}}^{\text{rel}} = 4$ (see Section above) gave the relative IV–CT absorbance of each species and the total IV–CT absorbance depending on the electric potential (Figure 7). It becomes clear from Figure 7 that the total IV–CT band displays its maximum absorbance at the potential ($E_{\text{pot}} = 0.484$ V) when $\mathbf{1}^{3+}$ has its approximate maximum concentration. From Figure 7 one can obtain the relative concentrations $c_{1^{i^{++}}}^{\text{rel}}$ of $\mathbf{1}^{2+}$, $\mathbf{1}^{3+}$, and $\mathbf{1}^{4+}$ at that potential. Together with the relative absorptivities $\epsilon_{1^{i^{++}}}^{\text{rel}}$, the maximal total integrated absorbance $F = 45.6 \text{ cm}^{-1}$, the total absorbance $E = 7.02 \times 10^{-3}$ of the experimental IV–CT band and the absorbance $E_{1^{++}}^0 = 0.887$ as well as the absorptivity $\epsilon_{1^{++}}^0 = 82\,000 \text{ M}^{-1} \text{ cm}^{-1}$ of $\mathbf{1}^+$ at 325 nm before oxidation, one can calculate the integrated absorptivities $A_{1^{i^{++}}}$ as well as the absolute molar absorptivities $\epsilon_{1^{i^{++}}} = \epsilon_{1^{i^{++}}}^{\text{rel}} \cdot \epsilon^0$ using eqs 10 and 11 which give $A_{1^{2+}} = A_{1^{4+}} = 4.00 \times 10^6 \text{ M}^{-1} \text{ cm}^{-2}$ and $A_{1^{3+}} = 5.33 \times 10^6 \text{ M}^{-1} \text{ cm}^{-1}$ and $\epsilon_{1^{2+}} = \epsilon_{1^{4+}} = 620 \text{ M}^{-1} \text{ cm}^{-1}$ and $\epsilon_{1^{3+}} = 820 \text{ M}^{-1} \text{ cm}^{-1}$. The quantities

$$A_{1^{i^{++}}} = \int \epsilon_{1^{i^{++}}} d\tilde{\nu} = \epsilon_{1^{i^{++}}}^{\text{rel}} \int \epsilon^0 d\tilde{\nu} = \frac{\epsilon_{1^{i^{++}}}^{\text{rel}} \cdot F \cdot \epsilon_{1^{++}}^0}{E_{1^{++}}^0 \cdot \sum_{i=1}^5 \epsilon_{1^{i^{++}}}^{\text{rel}} c_{1^{i^{++}}}^{\text{rel}}} \quad (10)$$

$$\epsilon^0 = \frac{E \cdot \epsilon_{1^{++}}^0}{E_{1^{++}}^0 \cdot \sum_{i=1}^5 \epsilon_{1^{i^{++}}}^{\text{rel}} c_{1^{i^{++}}}^{\text{rel}}} \quad (11)$$

measured and calculated by eqs 7 and 8 are collected in Table 2. The energy of the IV–CT band corresponds to the reorga-

TABLE 2: Optical Data for the IV–CT Band as Well as Calculated Electronic Coupling V

	$\tilde{\nu}_{\text{max}}$ [cm ⁻¹] ^a	ϵ [M ⁻¹ cm ⁻¹] ^b	$\tilde{\nu}_{1/2}$ (HTL) [cm ⁻¹] ^c	μ_{eg} [D] ^d	V [cm ⁻¹] ^e
$\mathbf{1}^{2+}$	11800	620	5210	1.76	260
$\mathbf{1}^{3+}$	11800	820	5210	2.04	260
$\mathbf{1}^{5+}$	11800	620	5210	1.76	260

^a ±500 cm⁻¹ ^b ±100 M⁻¹cm⁻¹ ^c ±100 cm⁻¹ ^d ±0.15 D ^e ±20 cm⁻¹

nization energy λ (11 800 cm⁻¹) which is significantly higher than in other linear and branched triarylamine systems (ca. 5500–9500 cm⁻¹).^{4q,5c,d,e} Whether this effect is due to a higher vibrational or solvent contribution to λ could in principle be elucidated by solvent dependent measurements.²⁵ However, this proved to be impossible owing to solubility problems and to the fact that the IV–CT band is partially hidden by the radical band at 800 nm which will presumably even be worse in more polar solvents than CH₂Cl₂. We assume that the crowded arrangement leads to an interlinking of solvent molecules sitting between the triarylamine branches which might increase the solvent contribution to λ . On the other hand, ion-pairing effects might also contribute to the higher reorganization energy.²⁶ These effects should be larger in the higher charged radical cations. However, we did not observe any significant changes of the IV–CT band shape during stepwise oxidation from $\mathbf{1}^{2+}$ to $\mathbf{1}^{4+}$. The electronic coupling ($V = 260 \text{ cm}^{-1}$) is about that of meta-phenylene bridged triarylamines ($V = 180\text{--}230 \text{ cm}^{-1}$) with an N–N distance of 12.5 Å.^{5c,d} The fact that $\mathbf{1}^+$ has a branched structure raises the question whether solvent molecules sitting between the branches mediate the ET, i.e., the ET occurs directly between the triarylamine centers, or whether the ET proceeds via the phosphorus center. Zimmt et al.²⁷ and Paddon-Row et al.²⁸ investigated donor/acceptor structures with rigid saturated spacers and found that for a U shaped spacer the ET occurs via the solvent molecules sitting between donor and acceptor. Although we have no proof, we also assume that this is true for the radical cations of $\mathbf{1}^+$, because cationic phosphorus centers are known to act as insulating bridges.²⁹

AM1 Calculation of the Coupling Energies. Previously, we have shown that AM1 calculations of the HOMO and HOMO-1 energies give a very good estimate of the coupling energy with $V(\text{AM1}) = [\epsilon(\text{HOMO-1}) - \epsilon(\text{HOMO})]/2$ for bridged bis-(triarylamine) systems.^{4q} The situation in $\mathbf{1}^+$ is somewhat more complex because the four highest occupied orbitals have to be used for the evaluation of V in $\mathbf{1}^+$. These highest occupied orbitals consist to a large extent (ca. 40%) of nitrogen lone pair orbitals in accordance with EPR measurements of triarylamine radical cations.³⁰ Because the correct molecular symmetry of $\mathbf{1}^+$ is S_4 there are two different coupling interactions V_1 and V_2 whose relative value depends on the orientation of the triarylamine moieties (the nitrogen lone-pair orbitals) relative to each other. According to Mislow et al.,³¹ the orientation of the phenyl rings in Ph₄X species can be defined by the dihedral angle φ between the plane of the phenyl ring (P–Ph–N) and the plane given by the P–N vector and the S_4 axis (Chart 5). While the AM1 optimization yielded P–C distances much too short (1.594 Å) in comparison with the X-ray structure (1.780 Å), a PM3 optimization gave the correct P–C distances (1.759 Å) but slightly pyramidal nitrogen centers. Thus, in the present case we used the PM3 parametrization for the energy calculations based on the X-ray coordinates (the C–H bonds were fixed at 1.09 Å) and varied the angle φ between 20° and 45°. The resulting PM3 HOMO eigenvalues were fitted by the eigenvalues $\epsilon_1 = H + V_1 + 2V_2$, $\epsilon_2 = \epsilon_3 = H - V_1$, and $\epsilon_4 = H +$

$$\begin{vmatrix} H - \epsilon & V_1 & V_2 & V_2 \\ V_1 & H - \epsilon & V_2 & V_2 \\ V_2 & V_2 & H - \epsilon & V_1 \\ V_2 & V_2 & V_1 & H - \epsilon \end{vmatrix} = 0 \quad (12)$$

$V_1 - 2V_2$ of a 4×4 secular equation (eq 12) with V_1 and V_2 being the off-diagonal elements whose values are collected in Table 3. Because the energy differences which were fitted to the PM3 HOMO energy values are $\epsilon_1 - \epsilon_2 = 2(V_2 + V_1)$ and $\epsilon_2 - \epsilon_4 = 2(V_2 - V_1)$ the sign of V_1 is positive but that of V_2 is indeterminate as to sign. For $\varphi = 26.44^\circ$ (the angle found in the X-ray structure) both coupling energies are almost equal (ca. 110 cm^{-1}); at larger angles φ , V_2 decreases strongly to ca. 15 cm^{-1} at 45° while V_1 only slightly changes to 91 cm^{-1} . Another way to define the relative orientation of the nitrogen lone-pair orbitals is to look at the dihedral angle between the planes given by two different nitrogen lone-pairs and the N–N vector. As there are two different N–N vectors in the S_4 arrangement there are two different dihedral angles ϑ_1 and ϑ_2 . While ϑ_2 is almost independent of φ yielding a fairly constant V_2 , ϑ_1 rises strongly to ca. 90° at $\varphi = 45^\circ$ thus minimizing the electronic interaction between this pair of nitrogen lone-pair orbitals. The fact that $V_1 = V_2$ at $\varphi = 26.44^\circ$ as found in the X-ray structure supports our simplification of approximate tetrahedral “electronic” geometry for $\mathbf{1}^+$ where $V_1 = V_2 = V$.

In contrast to their linear bis(triarylamine) systems where semiempirical calculations gave quantitatively correct results for V ,⁴⁴ the AM1 computed coupling energy ($V_1 \approx V_2 \approx 110 \text{ cm}^{-1}$) for $\mathbf{1}^+$ is much smaller than the experimental one (260 cm^{-1}).³² This might be due to neglected solvent effects because we assume solvent molecules to sit between the triarylamine branches mediating the ET.

Conclusions

A simple and highly symmetrical tetraorganophosphorus ion serves to illustrate how Marcus theory can be adopted to analyze multidimensional ET systems. While the thermal ET pathway is one-dimensional for $\mathbf{1}^{2+}$ and $\mathbf{1}^{4+}$ there exist two possibilities for $\mathbf{1}^{3+}$: a concerted two-dimensional process and a two-step one-dimensional way. The former leads over a hill top and, consequently, is forbidden. This interpretation is in agreement with the calculations by Guthrie if the site energies at intermediate corners are low (in our case they are at the same level as the starting and the end point). A two-dimensional photoexcited ET also is forbidden as this should be a two-photon excited process. This agrees with the generally accepted concept that two-electron transfer processes in electrochemistry actually comprise two consecutive one-electron-transfer steps. Besides its interesting ET properties, $\mathbf{1}^+$ shows strong quadratic (non-linear optical) polarizability in solution which is currently under investigation.³³

Experimental Section

Tris{4-[*N,N*-di(4-methoxyphenyl)amino]phenyl}phosphane: ⁿBuLi in hexanes (3.06 mL, 1.6 M, 4.85 mmol) was added to a solution of *N,N*-di(4-methoxyphenyl)-4-iodophenylamine³⁴ (1.90 g, 4.41 mmol) in Et₂O at -78°C . The solution was kept at -25°C for 30 min. A colorless precipitate formed. The solution was cooled to -78°C and PCl₃ (1.16 mL, 1.32 mmol) was added. A yellow solution formed. After further stirring for 1 h, the solution was allowed to warm to room temperature. The product formed as a colorless precipitate which was filtered off under nitrogen atmosphere. The product (1.1 g, 88%) was air-sensitive and was immediately used for quaternization. ¹H NMR (250 MHz, CD₂Cl₂): $\delta = 7.12\text{--}7.02$ (18H, two AA'

TABLE 3: Electronic Coupling V_1 and V_2 as Well as the Angles between the Nitrogen Lone-Pair Orbitals ϑ_1 and ϑ_2 Depending on the Angle φ Derived from PM3 Calculations

φ [°]	20	26.44	30	35	40	45
V_1 [cm ⁻¹]	104	107	93	70	43	15
V_2 [cm ⁻¹]	115	110	105	100	95	91
ϑ_1 [°]	30.7	46.0	54.3	65.4	75.5	90.1
ϑ_2 [°]	39.1	39.3	39.5	39.7	40.6	42.5

overlapped), 6.84–6.78 (18H, two BB' overlapped), 3.77 (s, 18H, methoxy). C₆₀H₅₄N₃O₆P [944.08].

Tetrakis{4-[*N,N*-di(4-methoxyphenyl)amino]phenyl}-phosphonium-tetrafluoroborate $\mathbf{1}^+\text{BF}_4^-$. Tris{4-[*N,N*-di(4-methoxyphenyl)amino]phenyl}phosphane (944 mg, 1.0 mmol), *N,N*-di(4-methoxyphenyl)-4-iodophenylamine³⁴ (474 mg, 1.1 mmol) and Pd(OAc)₂ (11 mg, 0.05 mmol) were stirred in 10 mL of oxygen free, nitrogen-saturated *p*-xylene under nitrogen atmosphere at 100°C for 20 h. A colorless precipitate formed. This precipitate was filtered off, washed with benzene, and dried in vacuo. ¹H NMR (400 MHz, CD₂Cl₂): $\delta = 7.22\text{--}7.16$ (m, 8H, AA', aminophenyl), 7.16–7.11 (m, 16H, AA', 4-methoxyphenyl), 6.93–6.88 (m, 16H, BB', 4-methoxyphenyl), 6.86–6.81 (m, 8H, BB', aminophenyl), 3.79 (s, 24H, methoxy). ¹³C NMR (100.6 MHz, CD₂Cl₂): $\delta = 158.3, 154.1$ (d, $J_{\text{C,P}} = 2.7$ Hz), 138.3, 135.2 (d, $J_{\text{C,P}} = 11.6$ Hz), 128.6, 116.9 (d, $J_{\text{C,P}} = 13.4$ Hz), 115.6, 106.3 (d, $J_{\text{C,P}} = 101.0$ Hz), 55.9. For counterion metathesis, the iodide salt was dissolved in a mixture of CH₂Cl₂/MeOH ~3:1. This solution was poured into a saturated solution of NaBF₄ in MeOH. Water was added and the organic layer was separated. After removal of the solvent, the residue was dissolved in pure CH₂Cl₂ and insoluble salts were filtered off. This procedure was repeated three times. In the last step the organic layer was dried over MgSO₄. After removal of the solvent, the residue was purified by flash chromatography on silica gel (first CH₂Cl₂ then CH₂Cl₂/MeOH 100:1). The product was precipitated from CH₂Cl₂ with MeOH to give 640 mg (48%) of violet crystals. Mp: $>390^\circ\text{C}$ Anal. calcd. for [C₈₀H₇₂N₄O₈P]⁺[BF₄]⁻·H₂O: [1353.27] C 71.00, H 5.36, N 4.14; found C 70.98, H 5.46, N 4.04. MS (PILSIMS): $m/z = 1247.4$ ($\mathbf{1}^+$).

X-ray Structure Analysis. A single crystal of $\mathbf{1}^+\text{BF}_4^-$ was mounted with a glass fiber on a Nonius diffractometer equipped with a CCD area detector and measured with monochromatic MoK α radiation at 173 K. Space group *I*₄/a, $a = 21.323(3) \text{ \AA}$, $c = 15.947(3) \text{ \AA}$, $V = 7251(2) \text{ \AA}^3$, $Z = 4$. Data were collected between $\Theta = 2.49$ and 23.09° , 4271 reflections collected, 2402 independent reflections, 237 parameters refined. The structure was solved by direct methods and refined by full-matrix least-squares on F^2 (Sheldrick, G. M.; SHELX-97, Program for refinement of crystal structures, University of Göttingen, 1997). All non-hydrogen atoms were refined anisotropically, the hydrogen atoms isotropically in idealized positions. RI ($I > 2\sigma(I)$) = 0.0833, $wR2$ (all data) = 0.226, $-0.277 < \Delta\rho < 0.278$ e \AA^{-3} , GOF = 1.347.

Cyclic Voltammetry. Cyclic voltammetry measurements were performed in dry and oxygen free CH₂Cl₂ with 0.1 M tetrabutylammonium hexafluorophosphate (TBAH) as the supporting electrolyte and with ca. 0.001 M substrate under a nitrogen inert gas atmosphere. A conventional three electrode setup was used with a platinum disk working electrode and a Ag/AgCl pseudo reference electrode. The redox potentials were referenced against internal ferrocene/ferrocenium (Fc/Fc⁺). The long-term reversibility of the processes was checked by performing multi-cycle thin-layer measurements at 10 mV s^{-1} . Digital simulation of the CV for $\mathbf{1}^+$ was done with DigiSim 2.1.³⁵ For this simulation, we assumed reversible behavior for

all redox processes. The simulation converged to a single set of redox potentials with an error ± 2 mV. Several attempts using different initial values resulted in the same set of optimized redox potentials.

Spectroelectrochemistry. The solution of the cyclic voltammetry experiment was transferred by a syringe into a spectroelectrochemical optical transparent thin-layer cell (optical path length of 100 μm with a gold minigrid working electrode) described in ref 19. UV/Vis/NIR spectra were recorded with a Perkin-Elmer Lambda 9 spectrometer while applying a constant potential to the solution in the thin-layer arrangement referenced against an Ag/AgCl electrode. The potential was increased in 30 mV steps, and spectra were recorded until all oxidative processes in CH_2Cl_2 were fully covered. Back reduction was also performed to prove reversibility of the whole process.

Semiempirical Calculations. Energy calculations of I^+ were done at the PM3 RHF level using the MOPAC97 program³⁶ using the fixed coordinates from the X-ray structure investigation with all C–H bonds fixed at 1.09 Å and varying φ angles.

Acknowledgment. We are grateful to the Fonds der Chemischen Industrie, the Deutsche Forschungsgemeinschaft (La 991/2-1), and especially to Prof. J. Daub for his kind support during the period of our work at Regensburg. We thank Dr. M. Zabel for preliminary measurements of I^+BF_4^- .

References and Notes

- (1) (a) Barbara, P. F.; Meyer, T. J.; Ratner, M. A. *J. Phys. Chem.* **1996**, *100*, 13148. (b) *Chem. Rev.* **1992**, *92*, 2, 369. This issue is devoted to ET processes in biologically relevant systems. (c) Willner, I.; Willner, B. *Top. Current Chem.* **1991**, *159*, 153.
- (2) Kosloff, R.; Ratner, M. A. *Israel J. Chem.* **1990**, *30*, 45.
- (3) (a) Creutz, C. *Prog. Inorg. Chem.* **1983**, *30*, 1. (b) Richardson, D. E.; Taube, H. *Coord. Chem. Rev.* **1984**, *60*, 107.
- (4) (a) Mazur, S.; Sreekumar, C.; Schroeder, A. H. *J. Am. Chem. Soc.* **1976**, *98*, 6713. (b) Schroeder, A. H.; Mazur, S. *J. Am. Chem. Soc.* **1978**, *100*, 7339. (c) Jozefiak, T. H.; Almlöf, J. E.; Feyereisen, M. W.; Miller, L. L. *J. Am. Chem. Soc.* **1989**, *111*, 4105. (d) Rak, S. F. R.; Miller, L. L. *J. Am. Chem. Soc.* **1992**, *114*, 1388. (e) Nelsen, S. F.; Chang, H.; Wolff, J. J.; Adamus, J. *J. Am. Chem. Soc.* **1993**, *115*, 12276. (f) Bonvoisin, J.; Launay, J.-P.; Rovira, C.; Veciana, J. *Angew. Chem.* **1994**, *33*, 2106. (g) Nelsen, S. F.; Adamus, J.; Wolff, J. J. *J. Am. Chem. Soc.* **1994**, *116*, 1589. (h) Lahli, K.; Moradpour, A.; Bowlas, C.; Menou, F.; Cassoux, P.; Bonvoisin, J.; Launay, J.-P.; Dive, G.; Dehareng, D. *J. Am. Chem. Soc.* **1995**, *117*, 9995. (i) Nelsen, S. F.; Ismagilov, R. F.; Powell, D. R. *J. Am. Chem. Soc.* **1996**, *118*, 6313. (j) Nelsen, S. F.; Ramm, M. T.; Wolff, J. J.; Powell, D. R. *J. Am. Chem. Soc.* **1997**, *119*, 6863. (k) Nelsen, S. F.; Trieber, D. A.; Wolff, J. J.; Powell, D. R.; Rogers-Crowley, S. *J. Am. Chem. Soc.* **1997**, *119*, 6873. (l) Nelsen, S. F.; Ismagilov, R. F.; Powell, D. R. *J. Am. Chem. Soc.* **1997**, *119*, 10213. (m) Nelsen, S. F.; Ismagilov, R. F.; Teki, Y. *J. Am. Chem. Soc.* **1998**, *120*, 2200. (n) Nelsen, S. F.; Ismagilov, R. F.; Powell, D. R. *J. Am. Chem. Soc.* **1998**, *120*, 1924. (o) Nelsen, S. F.; Tran, H. Q.; Nagy, M. A. *J. Am. Chem. Soc.* **1998**, *120*, 298. (p) Nelsen, S. F.; Ismagilov, R. F.; Trieber, D. A. *Science* **1997**, *278*, 846. (q) Lambert, C.; Nöll, G. *J. Am. Chem. Soc.* **1999**, *121*, 8434. (r) Rovira, C.; Ruiz-Molina, D.; Elsner, O.; Vidal-Gancedo, J.; Bonvoisin, J.; Launay, J.-P.; Veciana, J. *Chem. Eur. J.* **2001**, *7*, 240.
- (5) (a) Haga, M.; Ali, M.; Sato, H.; Monjushiro, H.; Nozaki, K.; Kano, K. *Inorg. Chem.* **1998**, *37*, 2320. (b) Aoki, K.; Chen, J.; Haga, M. *J. Electroanal. Chem.* **1995**, *396*, 309. (c) Bonvoisin, J.; Launay, J.-P.; Van der Auweraer, M.; De Schryver, F. C. *J. Phys. Chem.* **1994**, *98*, 5052; see correction *J. Phys. Chem.* **1996**, *100*, 18006. (d) Bonvoisin, J.; Launay, J.-P.; Verbouwe, W.; Van der Auweraer, M.; De Schryver, F. C. *J. Phys. Chem.* **1996**, *100*, 17079. (e) Lambert, C.; Nöll, G. *Angew. Chem., Int. Ed.* **1998**, *37*, 2107. (f) Lambert, C.; Gaschler, W.; Schmälzlin, E.; Meerholz, K.; Bräuchle, C. *J. Chem. Soc., Perkin Trans. 2*, **1999**, 577.
- (6) (a) Huber, R. *Angew. Chem.* **1989**, *101*, 849. (b) Deisenhofer, J.; Michel, H. *Angew. Chem.* **1989**, *101*, 872.
- (7) (a) Marcus, R. A.; Sutin, N. *Biochim. Biophys. Acta* **1985**, *811*, 265. (b) Marcus, R. A. *Angew. Chem.* **1993**, *105*, 1161.
- (8) (a) Sutin, N. *Prog. Inorg. Chem.* **1983**, *30*, 441. (b) Creutz, C.; Newton, M. D.; Sutin, N. *J. Photochem. Photobiol. A* **1994**, *82*, 47. (c) Cave, R. J.; Newton, M. D. *Chem. Phys. Lett.* **1996**, *249*, 15. (d) Matyushov, D. V.; Ladanyi, B. M. *J. Phys. Chem. A* **1998**, *102*, 5027. (e) Newton, M. D. *Adv. Chem. Phys.* **1999**, *106*, 303.
- (9) Grunwald, E. *J. Am. Chem. Soc.* **1985**, *107*, 125.
- (10) Guthrie, J. P. *J. Am. Chem. Soc.* **1996**, *118*, 12878.
- (11) S. Nelsen applied the adequate theory for investigating a one-dimensional ET process where a bridge state is involved: see ref 4n.
- (12) (a) Stolka, M.; Yanus, J. F.; Pai, D. M. *J. Phys. Chem.* **1984**, *88*, 4707. (b) Pai, D. M.; Yanus, J. F.; Stolka, M. *J. Phys. Chem.* **1984**, *88*, 4714. (c) Borsenberger, P. M.; Weiss, D. S. *Organic Photoreceptors for Imaging Systems*, Marcel Dekker: New York, 1993. (d) Chen, C. H.; Tang, C. W. *Macromol. Symp.* **1997**, *125*, 1. (e) Katsuma, K.; Shirota, Y. *Adv. Mater.* **1998**, *10*, 223. (f) Thelakkat, M.; Schmidt, H.-W. *Adv. Mater.* **1998**, *10*, 219. (g) Selby, T. D.; Blackstock, S. C. *J. Am. Chem. Soc.* **1998**, *120*, 12155. (h) Koene, B. E.; Loy, D. E.; Thompson, M. E. *Chem. Mater.* **1998**, *10*, 2235. (i) Hu, N.-X.; Xie, S.; Popovic, Z.; Ong, B.; Hor, A.-M.; Wang, S. *J. Am. Chem. Soc.* **1999**, *121*, 5097. (j) Goodson, F. E.; Hauck, S. I.; Hartwig, J. F. *J. Am. Chem. Soc.* **1999**, *121*, 7527. (k) Wu, I.-Y.; Lin, J. T.; Tao, Y.-T.; Balasubramanian, E. *Adv. Mater.* **2000**, *12*, 668.
- (13) (a) Stickley, K. R.; Blackstock, S. C.; *Tetrahedron Lett.* **1995**, *36*, 1585. (b) Wienk, M. M.; Janssen, R. A. J. *J. Am. Chem. Soc.* **1997**, *119*, 4492. (c) Okada, K.; Imakura, T.; Oda, M.; Kajiwara, A.; Kamachi, M.; Sato, K.; Shiomi, D.; Taku, T.; Itoh, K.; Gherghel, L.; Baumgarten, M. *J. Chem. Soc., Perkin Trans 2*, **1997**, 1059. (d) Michinobu, T.; Takahashi, M.; Tsuchida, E.; Nishide, H. *Chem. Mater.* **1999**, *11*, 1969. (e) Ito, A.; Ono, Y.; Tanaka, K. *Angew. Chem.* **2000**, *112*, 1114.
- (14) For crystal structures of triarylaminines, see e.g. (a) Sobolev, A. N.; Bel'skii, V. K.; Romm, I. P.; Chernikova, N. Yu.; Guryanova, E. N. *Acta Crystallogr., Sect. C: Cryst. Struct. Commun.* **1995**, *C41*, 967. For a crystal structure of a triarylamine radical cation, see e.g. (b) Brown, G. M.; Freeman, G. R.; Walter, R. I. *J. Am. Chem. Soc.* **1977**, *99*, 6910.
- (15) We used Maple V release 5 for solving the secular equations.
- (16) For simplicity, we used quadratic potentials although it is well-known by the work of S. Nelsen that in some cases quartic augmented functions allow better simulation of the observed IV–CT spectra; see ref 4l.
- (17) In the borderline case of infinitely small coupling the minima of the adiabatic and the diabatic functions coincide. With increasing coupling, the minima of the diabatic hypersurface move towards each other. We refrained from a numeric search for the true minimum positions as this is quite laborious and these points will not deviate much from the one of the diabatic functions as can be seen from Figures 2 and 4.
- (18) Flanagan, J. B.; Margel, S.; Bard, A. J.; Anson, F. C. *J. Am. Chem. Soc.* **1978**, *100*, 4248.
- (19) Salbeck, J. *Anal. Chem.* **1993**, *65*, 2169.
- (20) (a) Hush, N. S. *Electrochim. Acta* **1968**, *13*, 1005. (b) Hush, N. S. *Coord. Chem. Rev.* **1985**, *64*, 135.
- (21) Robin, M.; Day, P. *Adv. Inorg. Radiochem.* **1967**, *10*, 247.
- (22) Bonvoisin et al. employed a more accurate band deconvolution which does not imply the same band shape and band maxima for differently charged species, see refs 5c and d. In our case, the bad signal-to-noise ratio as well as the fact that the IV–CT band strongly overlaps with a much stronger radical band prohibits this type of deconvolution. However, for weakly coupled species one can safely assume that the band shapes and maxima differ only marginally between differently charged species.
- (23) For a short discussion of the use of the N–N separation as the effective ET distance, see ref 4q.
- (24) Nelsen, S. F.; Newton, M. D. *J. Phys. Chem. A* **2000**, *104*, 10023.
- (25) Nelsen, S. F.; Tran, H. Q. *J. Phys. Chem. A* **1999**, *103*, 8139.
- (26) Nelsen, S. F.; Ismagilov, R. F. *J. Phys. Chem. A* **1999**, *103*, 5373.
- (27) (a) Cave, R. J.; Newton, M. D.; Kumar, K.; Zimmt, M. B. *J. Phys. Chem.* **1995**, *99*, 17501. (b) Kumar, K.; Lin, K. Z.; Waldeck, D. H.; Zimmt, M. B. *J. Am. Chem. Soc.* **1996**, *118*, 243. (c) Kumar, K.; Kurnikov, I. V.; Beratan, D. N.; Waldeck, D. H.; Zimmt, M. B. *J. Phys. Chem. A* **1998**, *102*, 5529. (d) Han, H.; Zimmt, M. B. *J. Am. Chem. Soc.* **1998**, *120*, 8001. (e) Read, I.; Napper, A.; Kaplan, R.; Zimmt, M. B.; Waldeck, D. H. *J. Am. Chem. Soc.* **1999**, *121*, 10976.
- (28) (a) Lawson, J. M.; Paddon-Row, M. N.; Schuddeboom, W.; Warman, J. M.; Clayton, A. H. A.; Ghiggino, K. P. *J. Phys. Chem.* **1993**, *97*, 13099. (b) Roest, M. R.; Verhoeven, J. W.; Schuddeboom, W.; Warman, J. M.; Lawson, J. M.; Paddon-Row, M. N. *J. Am. Chem. Soc.* **1996**, *118*, 1762. (c) Jolliffe, K. A.; Bell, T. D. M.; Ghiggino, K. P.; Langford, S. J.; Paddon-Row, M. N. *Angew. Chem., Int. Ed. Engl.* **1998**, *37*, 916.
- (29) (a) Schiemenz, G. P. *Phosphorus* **1973**, *3*, 125. (b) Horner, L.; Duda, U.-M. *Phosphorus* **1975**, *5*, 109.
- (30) Neugebauer, F. A.; Bamberger, S.; Groh, W. R. *Chem. Ber.* **1975**, *108*, 2406.
- (31) Hutchings, M. G.; Andose, J. D.; Mislow, K. *J. Am. Chem. Soc.* **1975**, *97*, 4553.
- (32) Prof. S. Nelsen (private communication) also observed that AM1 calculations underestimate the coupling for saturated-bridge systems.
- (33) Bourgoigne, C.; Le Fur, Y.; Juen, P.; Masson, P.; Nicoud, J.-F.; Masse, R. *Chem. Mater.* **2000**, *12*, 1025.
- (34) Lambert, C.; Nöll, G.; Schmälzlin, E.; Meerholz, K.; Bräuchle, C. *Chem. Eur. J.* **1998**, *4*, 2129.
- (35) Rudolph, M. Feldberg, S. W.; DigiSim 2.1, Bioanalytical Systems, Inc. 1996.
- (36) Mopac97, Fujitsu Inc. 1997.